


## Crystal structure of calcium vanadate-phosphate fluoride

Z. L. Dong <sup>a)</sup> and T. J. White

Nanyang Technological University, 50 Nanyang Avenue, Singapore 639798, Singapore

(Received 10 September 2018; accepted 28 January 2019)

Apatite-type materials  $A_4A''_6(BO_4)_6X_2$  have two unique cations sites  $A^I$  and  $A^{II}$ , which can host large mono-, di- tri- and tetra-valent cations. The average cation radii will affect the twist angle and lattice constants. However, there are few reports on the influence of B site substitutions on the twist angle and lattice parameters. It is believed that the lattice constant variation as a function of B site substitutions may not follow the same twist-angle model as proposed for A site. This work reports our results on the crystal chemistry of synthetic apatite  $Ca_{10}(V_xP_{1-x}O_4)_6F_2$  obtained through the crystal structure characterization using Rietveld refinement and high-resolution transmission electron microscopy. The quantification of vanadium/phosphorus partitioning in  $BO_4$  tetrahedra showed that equilibrium with more than 70% substitution of phosphorous by vanadium was difficult to achieve unless longer annealing (about 1 week at 900 °C) was employed. In comparison with the apatites with different ionic radii at  $A^I$  and  $A^{II}$  sites,  $Ca_{10}(V_xP_{1-x}O_4)_6F_2$  apatites with different ionic radii at B site show little twist angle variation for the whole series, which indicates that the dilation of unit cell constants is mainly because of the expansions of  $BO_4$  tetrahedra when A site cation is fixed. © 2019 International Centre for Diffraction Data. [doi:10.1017/S0885715619000150]

Key words: apatite, Rietveld refinement, twist angles, high-resolution transmission electron microscopy

## I. INTRODUCTION

Apatite-type materials can be used in the areas of bone replacement (Hench, 1991), catalysis (Choudary *et al.*, 2005), environmental remediation (Chen *et al.*, 1997), ultrafast lasers (Druon *et al.*, 2002), and ionic conductors (Arikawa *et al.*, 2000) depending on their chemical compositions. The control of cation site occupancy in apatite-type materials is of great importance for tuning their properties. With the aid of powder X-ray diffraction (XRD), Rietveld refinement, and high-resolution microscopy imaging techniques, it is possible to retrieve information on cation order-disorder, and cation site occupancies of apatite-type ceramics.

In our previous studies (White and Dong, 2003; Shen *et al.*, 2010), issues related to  $A^I$  and  $A^{II}$  site crystallography in  $A_4A''_6(BO_4)_6X_2$  apatite was discussed in detail. Here  $A^I$  and  $A^{II}$  are cation sites with different symmetries.  $BO_4$  is the tetrahedron site and X is the anion site in the channel.

As  $A^I$  and  $A^{II}$  sites have a different size as well as the chemical environment, when two or more kinds of atoms occupy the A sites, the bigger atoms tend to enter  $A^{II}$  preferentially (Dong and White, 2004a, 2004b). Longer annealing time is needed in order to achieve the equilibrium during the cation migration process. An example is the Pb/Ca substitution at  $A^I$  and  $A^{II}$  sites. More than 2 weeks annealing at 800 °C is required to establish the equilibrium occupancies of Ca/Pb in both  $A^I$  and  $A^{II}$  sites. When the composition and average ionic radii of  $A^I$  site changes, the twist angle of the  $A^I$

metaprism will change. The twisting of the metaprism will vary the lattice constants (White and Dong, 2003).

For B site substitution, studies are very limited in comparison with that of A sites. B is in the centre of a tetrahedron site, having the same symmetry as the  $A^{II}$  site for apatites with  $P6_3/m$  space group. When B sites are forced to fill with two or more kinds of atoms in synthetic apatites, the formation of equilibrium  $BO_4$  tetrahedron net may require higher temperature or longer time. There is also possibility of forming an ordering structure of  $BO_4$  polyhedra. In our previous research, endeavour has been made to incorporate V atoms into  $PO_4$  tetrahedra (Dong *et al.*, 2003; Mercier *et al.*, 2007; Dong and White, 2008; Dong, 2009; Lu *et al.*, 2013). Ca and F are chosen to fill the  $A^I$ ,  $A^{II}$  and X sites as calcium-fluorine apatites are well studied and understood.

In this study, X-ray Rietveld refinement and high-resolution transmission electron microscopy (HRTEM) are used as the fundamental tools to study the crystal structure of  $Ca_{10}(V_xP_{1-x}O_4)_6F_2$  apatites. The structure description by a twist angle of  $A^I$ - $O_6$  metaprism are used, which can help understand the lattice constant variation in relation with B site size.

## II. EXPERIMENTAL

Apatite minerals used for the present study were synthesized via chemical reaction route. CaO obtained by firing and decomposing AR grade  $CaCO_3$  at 900 °C,  $V_2O_5$  and  $CaF_2$  powders were mixed in stoichiometric proportions in diluted orthophosphoric acid and stirred for more than 2 h. For different  $Ca_{10}(V_{1-x}P_xO_4)_6F_2$  samples with different x values, different amount of orthophosphoric acid with 85%

<sup>a)</sup> Author to whom correspondence should be addressed. Electronic mail: zldong@ntu.edu.sg

concentration was transferred into a beaker, after which deionized water was added to reach a 75 ml for each diluted solution. The sludge was dried at about 95 °C in an oven for 2 days, followed by heat treatment at 900 °C for 24 h. Powder XRD patterns were collected using a Siemens D5005 X-ray diffractometer fitted with Cu-tube that was operated at 40 kV and 40 mA. Divergence slit, anti-scatter slit, receiving slit and detector slit of 0.5°, 0.5°, 0.1 mm and 0.6 mm were aligned. Primary soller slit in the incident path and secondary soller slit in the diffracted path were used to limit the beam divergence along the longitude of the above slits within 2.3°. Scans were collected from 10° to 140°2θ with a step size 0.01°, and counting time 5 s per step. Under these conditions the intensity of the strongest peak was 1500–2000 counts. Prior to data collection, the fired conglomerations were mechanically ground to fine powders to minimize crystal size effects. The XRD patterns were refined using Bruker Topas 2.1 Rietveld program with fundamental parameters approach (Cheary and Coelho, 1992, 1998). For each compound four polynomial background co-efficient and peak shift because of zero error and sample displacement were refined. As no crystallographic data could be located for the complete series  $\text{Ca}_{10}(\text{V}_x\text{P}_{1-x}\text{O}_4)_6\text{F}_2$ , the starting model for refinement used the atomic positions from  $\text{Ca}_{10}(\text{PO}_4)_6\text{F}_2$ . (Sudarsanan *et al.*, 1972). For each model the occupancies of V and P at B site were refined. B-O bond length restrains ( $B\text{-O} = 1.54 + 0.2x \text{ \AA}$  was proposed for  $\text{Ca}_{10}(\text{V}_x\text{P}_{1-x}\text{O}_4)_6\text{F}_2$ ) ranging from 1.54 Å to 1.74 Å in the tetrahedra were applied to ensure the V/P-O bond lengths within a reasonable range. Patterns were analysed systematically from the phosphorus to vanadium endmembers. For apatite samples with  $x$  higher than 0.7 in  $\text{Ca}_{10}(\text{V}_x\text{P}_{1-x}\text{O}_4)_6\text{F}_2$  series, sintering at 900 °C for 24 h is not sufficient to reach the equilibrium as indicated by the XRD patterns and high  $R_{\text{Bragg}}$  values. For those samples, further annealing at 900 °C for 1 week was conducted.

TEM powder specimens were prepared by dispersing a small quantity of powders in ethanol under an ultrasonic bath for a few minutes, followed by dropping the suspension onto a holey-carbon coated copper-grid. HRTEM study was carried out in a JEOL JEM-3010 microscope operated under 300 kV. A Gatan double tilt holder was employed in order that a particular orientation could be found by tilting.

### III. RESULTS AND DISCUSSIONS

#### A. Variations of unit cell parameters with chemical compositions

The lattice parameters of 11 apatite  $\text{Ca}_{10}(\text{V}_x\text{P}_{1-x}\text{O}_4)_6\text{F}_2$  with  $x$  ranging from 0 to 1 were obtained by refining the XRD pattern using the Rietveld method. It was realized that the V occupancies in B site could deviate from stoichiometric compositions in the apatite series especially for higher V apatites  $\text{Ca}_{10}(\text{V}_{0.8}\text{P}_{0.2}\text{O}_4)_6\text{F}_2$  and  $\text{Ca}_{10}(\text{V}_{0.9}\text{P}_{0.1}\text{O}_4)_6\text{F}_2$ . The structure of the endmember  $\text{Ca}_{10}(\text{VO}_4)_6\text{F}_2$  were presented earlier (Dong and White, 2004b) and it displayed  $P2_1/m$  symmetry. In our analysis, the series of apatites between the two end members  $\text{Ca}_{10}(\text{PO}_4)_6\text{F}_2$  and  $\text{Ca}_{10}(\text{VO}_4)_6\text{F}_2$  were displaying  $P6_3/m$  symmetry. As we did not synthesize apatites  $\text{Ca}_{10}(\text{V}_{1-x}\text{P}_x\text{O}_4)_6\text{F}_2$  with  $0.9 < x < 1.0$ , we are not sure whether there are monoclinic apatites with  $P2_1/m$  symmetry within this composition range.

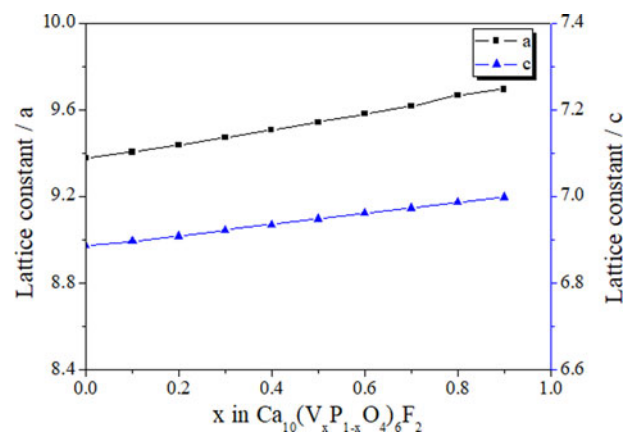


Figure 1. (Color online) Variation of lattice constants with vanadium content at B site for  $\text{Ca}_{10}(\text{V}_x\text{P}_{1-x}\text{O}_4)_6\text{F}_2$  ( $x = 0, 1, \dots, 9$ ).

The unit cell parameters for the apatites are shown in Figure 1. Twist angles that were calculated based on the  $A^I$ ,  $O_1$  and  $O_2$  atom positions (White and Dong, 2003) and the B-O bond lengths obtained from Rietveld refinement are shown in Table I. As oxygen coordinates are only uncertain in the 3rd or 4th decimal place, the accuracy of  $<0.1^\circ$  for the twist angles can be achieved. Unlike the series of  $\text{Pb}_x\text{Ca}_{10-x}(\text{VO}_4)_6\text{F}_2$  apatites with the twist angle changing systematically as  $a$  and  $c$  change, the twist angles for series  $\text{Ca}_{10}(\text{V}_x\text{P}_{1-x}\text{O}_4)_6\text{F}_2$  have very limited changes from one member to another, except for the  $\text{Ca}_{10}(\text{V}_{0.9}\text{P}_{0.1}\text{O}_4)_6\text{F}_2$  apatite that shows a value slightly lower than  $23.0^\circ$ . The projected apatite structure showing the twist angle is presented in Figure 2. The bond length values of  $A^I\text{-O}1$  or  $A^I\text{-O}2$  are within a relative narrow range, showing no trends of variation. The  $A^{II}\text{-O}1$  distance increases when B-O bond length increases from lower to higher V concentration as calculated from the results obtained (Dong, 2009).

Our previous studies reveal that in A site substitution apatites, the composition of  $A^I$  and  $A^{II}$  sites will determine the twisting of  $A^I\text{O}_6$  metaprism (White and Dong, 2003), and consequently the values of lattice parameter  $a$  and  $c$ . The metaprism collapses more severely by twisting when A site filled with smaller atoms.

In this work, as V content in B site increases, the tetrahedron expands, and that will cause the lattice to dilate. The V-O1, V-O2 and V-O3 bond lengths in Table I imply that the tetrahedron expands isotropically, leading to the expansions of lattice constants  $a$  and  $c$ . The lattice constants  $a$  and  $c$  of the apatites vary almost linearly with B site composition in  $\text{Ca}_{10}(\text{V}_x\text{P}_{1-x}\text{O}_4)_6\text{F}_2$  apatites as shown in Figure 1. More detailed crystallographic data are given in the Supplementary Material.

#### B. HRTEM of $\text{Ca}_{10}(\text{V}_x\text{P}_{1-x}\text{O}_4)_6\text{F}_2$ apatite

The refinement results from XRD data were used as average structures for HRTEM characterization. As each of the powder samples has a different V/P ratio, HRTEM imaging would show different contrast with the tetrahedra net. Through studying the projected lattice structure, it seems that the  $[2-1-10]$  orientation can show the alignment of  $\text{BO}_4$  tetrahedra nicely.

Figure 3 are experimental HRTEM images from  $\text{Ca}_{10}(\text{V}_{0.7}\text{P}_{0.3}\text{O}_4)_6\text{F}_2$  apatite from directions  $[2-1-10]$  and  $[0001]$ . The sample is not as beam-sensitive in comparison

TABLE I. Unit cell parameters, twist angles and average  $B-O$  bond lengths for  $\text{Ca}_{10}(\text{V}_x\text{P}_{1-x}\text{O}_4)_6\text{F}_2$  ( $x=0, 1, \dots, 9$ ).

Composition: $x$	0	0.1	0.2	0.3	0.4	0.5	0.6	0.7	0.8	0.9
$a$ (Å)	9.3752(1)	9.4044(8)	9.4354(2)	9.4725(2)	9.5080(2)	9.5427(2)	9.5799(3)	9.6164(20)	9.6669(13)	9.6942(5)
$c$ (Å)	6.8862(1)	6.8965(6)	6.9081(2)	6.9222(2)	6.9348(2)	6.9479(2)	6.9612(2)	6.9729(15)	6.9862(10)	6.9976(4)
Twist angle	24.1	24.1	23.8	24.4	24.1	24.1	23.0	23.8	23.5	22.9
V/P-O average	1.555	1.561	1.577	1.593	1.612	1.631	1.648	1.666	1.686	1.704

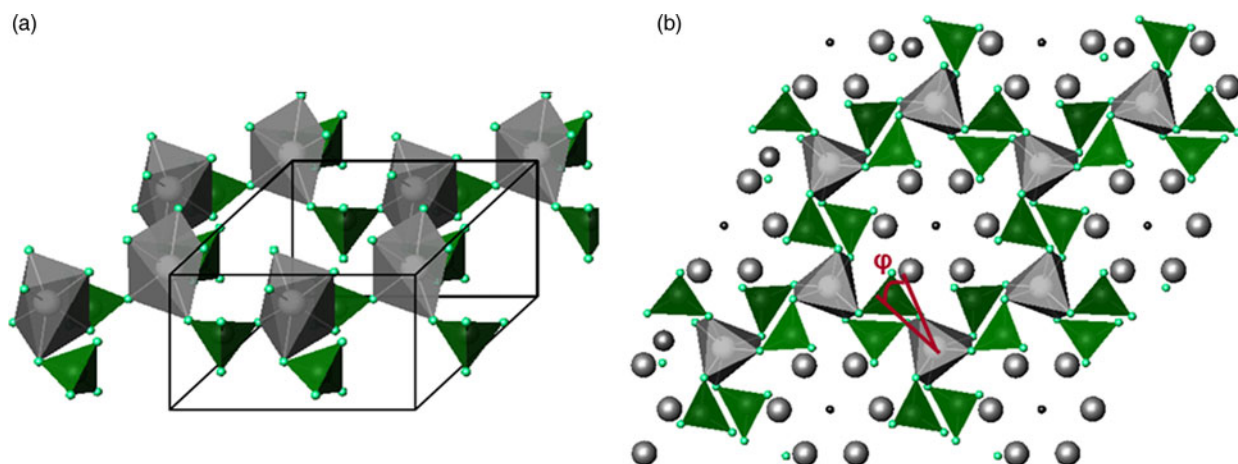


Figure 2. Twist angle in apatite structure. (a) A1-O6 octahedra formed by twisting prisms, (b) projected structure of A1-O6 octahedra showing the twist angle.

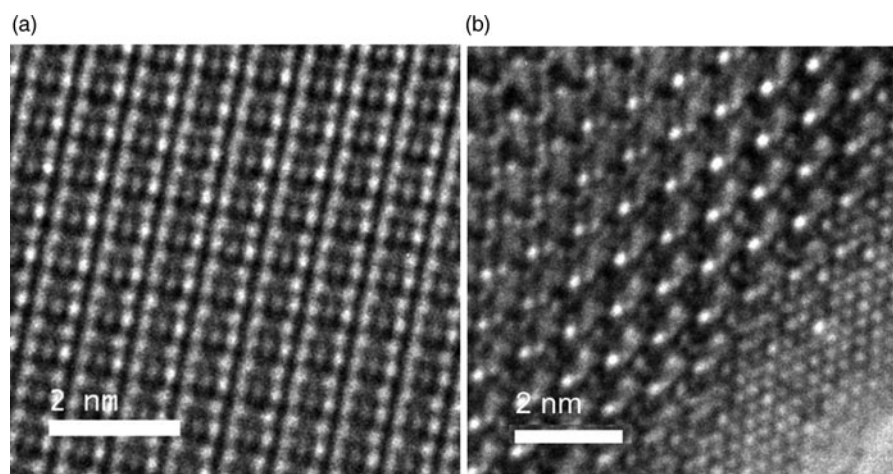


Figure 3. HRTEM images of  $\text{Ca}_{10}(\text{V}_{0.7}\text{P}_{0.3}\text{O}_4)_6\text{F}_2$  apatite (a) from zone axis  $[2-1-1\ 0]$ , and (b) from zone axis  $[0001]$ .

with pure P apatite, and its projected structure looks very homogeneous.

Although our conventional HRTEM observation did not reveal  $B$  site ordered structure, it is still interesting to consider how the HRTEM images may look like if ordering occurs. Therefore, we propose to use Cs-corrected high-resolution transmission electron microscope in our future experiments to examine the features of alignment of  $\text{BO}_4$  tetrahedra. An exemplar apatite is  $\text{Ca}_{10}(\text{V}_{0.7}\text{P}_{0.3}\text{O}_4)_6\text{F}_2$ , which has a stoichiometric composition of 0.70 V. The refinement result shows that the V occupancy is 0.78, which is close to 75%. If we assume that vanadium occupy the whole layer of  $z=1/4$ , and half layer of  $z=3/4$ , and phosphors occupy the other half layer of  $z=3/4$ , we should be able to simulate the HRTEM image from  $[2-1-10]$  direction, and further examine the projected structure using Cs-corrected HRTEM to clarify whether this particular apatite displays  $B$  site ordering.

#### IV. CONCLUSIONS

The  $\text{Ca}_{10}(\text{V}_x\text{P}_{1-x}\text{O}_4)_6\text{F}_2$  apatites were synthesized through solid-state reactions, and their microstructures were characterized by X-Ray Rietveld refinement and HRTEM. The changes of  $B$  site occupancies do not obviously vary the twist angle of  $A'O_6$  metaprism. The dilation of lattice parameters  $a$  and  $c$  is mainly because of the expansion of  $\text{BO}_4$  tetrahedra when V occupancy increases. For  $\text{Ca}_{10}(\text{V}_x\text{P}_{1-x}\text{O}_4)_6\text{F}_2$  apatites, no tetrahedra ordering along the  $c$ -axis is observed using conventional high-resolution electron microscopy.

#### SUPPLEMENTARY MATERIAL

The supplementary material for this article can be found at <https://doi.org/10.1017/S0885715619000150>

## ACKNOWLEDGEMENTS

The authors would like to thank Ms Lim Suo Hong from former Environmental Technology Institute for her help on heat treatment of powder samples. This work was supported through A\*STAR Grant 012 105 0123.

- Arikawa, H., Nishiguchi, H., Ishihara, T. and Takita, Y. (2000). "Oxide ion conductivity in Sr-doped  $\text{La}_{10}\text{Ge}_6\text{O}_{27}$  apatite oxide," *Solid State Ionics*, **136–137**, 31–37.
- Cheary, R. W. and Coelho, A. A. (1992). "A fundamental parameters approach to X-ray line-profile fitting," *J. Appl. Cryst.* **25**, 109–121.
- Cheary, R. W. and Coelho, A. A. (1998). "Axial divergence in a conventional X-ray powder diffractometer. I. Theoretical foundations," *J. Appl. Cryst.* **31**, 851–861.
- Chen, X. B., Wright, J. V., Conca, J. L. and Peurrung, M. L. (1997). "Effects of pH on heavy metal sorption on mineral apatite," *Environ. Sci. Technol.* **31** (3), 624–631.
- Choudary, B. M., Sridhar, C., Kantam, M. L., Venkanna, G. T. and Sreedhar, B. (2005). "Design and evolution of copper apatite catalysts for N-arylation of heterocycles with chloro- and fluoroarenes," *J. Am. Chem. Soc.* **127**, 9948–9949.
- Dong, Z. L. (2009). "X-ray diffraction, Rietveld crystal structure refinement and high-resolution transmission electron microscopy of nano-structured materials," in *Handbook of Nanoceramics and Their Based Nanodevices*, edited by Tseung-Yuen Tseng and Hari Singh Nalwa (American Scientific Publishers, California), Vol. **3**, pp. 303–336.
- Dong, Z. L. and White, T. J. (2004a). "Calcium–lead fluoro-vanadinite apatites. I. Disequilibrium structures," *Acta Crystallogr., Sect. B: Struct. Sci.* **60**, 138–145.
- Dong, Z. L. and White, T. J. (2004b). "Calcium–lead fluoro-vanadinite apatites. II. Equilibrium structures," *Acta Crystallogr., Sect. B: Struct. Sci.* **60**, 146–154.
- Dong, Z. L. and White, T. J. (2008). "Solid state synthesis and crystal structure of  $\text{Ca}_{10}(\text{V}_x\text{P}_{1-x}\text{O}_4)_6\text{F}_2$  apatite," *Microsc. Microanal.* **14** (Suppl 2), 210–211.
- Dong, Z. L., Kim, J., Lim, S. H., Laursen, K. and White, T. J. (2003). "Crystal Structure of  $\text{Ca}_{10}(\text{V}_x\text{P}_{1-x}\text{O}_4)_6\text{F}_2$  Apatite Synthesised via Solid State Reaction", Proceedings of the 2nd International Conference on Materials for Advanced Technologies, MRS Singapore, p. 736.
- Druon, F., Chenais, S., Raybaut, P., Balembos, F., Georges, P., Gaume, R., Haumesser, P. H., Viana, B., Vivien, D., Dhellemmes, S., Ortiz, V. and Larat, C. (2002). "Apatite-structure crystal,  $\text{Yb}^{3+}$ :  $\text{SrY}_4(\text{SiO}_4)_3\text{O}$ , for the development of diode-pumped femtosecond lasers," *Opt. Lett.* **27** (21), 1914–1916.
- Hench, L. L. (1991). "Bioceramics: from concept to clinic," *J. Am. Ceram. Soc.* **74** (7), 1487–1510.
- Lu, F. Y., Dong, Z. L., Zhang, J. M., White, T. J., Ewing, R. C. and Lian, J. (2013). "Tailoring the radiation tolerance of vanadate-phosphate fluorapatites by chemical composition control," *RSC Adv.* **3**, 15178–15184.
- Mercier, P. H. J., Dong, Z. L., Baikie, T., Page, Y. L., White, T. J., Whitfield, P. S. and Mitchel, L. D. (2007). "Ab initio constrained crystal-chemical Rietveld refinement of  $\text{Ca}_{10}(\text{V}_x\text{P}_{1-x}\text{O}_4)_6\text{F}_2$  apatites," *Acta Crystallogr., Sect. B: Struct. Sci.* **63**, 37–48.
- Shen, Y. Q., Chen, R., Sun, H. D., Tok, A. and Dong, Z. L. (2010). "Study of the cation distributions in Eu doped  $\text{Sr}_2\text{Y}_8(\text{SiO}_4)_6\text{O}_2$  by X-ray diffraction and photoluminescent spectra," *J. Solid State Chem.* **183**, 3093–3099.
- Sudarsanan, K., Mackie, P. E. and Young, R. A. (1972). "Comparison of synthetic and mineral fluoroapatite,  $\text{Ca}_5(\text{PO}_4)_3\text{F}$ , in crystallographic detail," *Mater. Res. Bull.* **1**, 1331–1338.
- White, T. J. and Dong, Z. L. (2003). "Structural derivation and crystal chemistry of apatites," *Acta Crystallogr., Sect. B: Struct. Sci.* **59** (1), 1–16.